aPKC-mediated displacement and actomyosin-mediated retention polarize Miranda in *Drosophila* neuroblasts

Matthew Hannaford[1], Anne Ramat[1] , Nicolas Loyer[1] and Jens Januschke[1#]

[1]Cell & Developmental Biology, School of Life Sciences, University of Dundee, Dundee, UK

correspondence: j.januschke@dundee.ac.uk

SUMMARY

Cell fate generation can rely on the unequal distribution of molecules during progenitor cell division in the nervous system of vertebrates and invertebrates. Here we address asymmetric fate determinant localization in the developing *Drosophila* nervous system, focusing on the control of asymmetric Miranda distribution in mitotic larval neuroblasts. Two models have been put forward to explain Miranda asymmetry. One proposed that actomyosin drives basal Miranda localization. Later, it was proposed that spatially controlled aPKC dependent phosphorylation of Mira can explain its polarized localization. We reveal now that both the actomyosin network and aPKC phosphorylation of Miranda are required, but operate at distinct phases of the cell cycle. Using live imaging of neuroblast polarity reporters at endogenous levels of expression we show that displacement of Miranda by phospho-regulation by aPKC at the onset of mitosis and differential binding to the actomyosin cortex after nuclear envelope breakdown establishes asymmetric Miranda localization.

INTRODUCTION

The development of the central nervous system depends on asymmetric cell divisions for the balanced production of progenitor as well as differentiating cells. During vertebrate and invertebrate neurogenesis, cell fates can be established through the unequal inheritance of cortical domains or fate determinants during asymmetric progenitor divisions (Knoblich 2008; Doe 2008; Marthiens & ffrench-Constant 2009; Alexandre et al. 2010).

An important step in asymmetric cell division is the establishment of a polarity axis, which is crucial to coordinate unequal fate determinant segregation. Asymmetrically dividing *Drosophila* neuroblasts (NBs) establish an axis of polarity at the onset of mitosis. Like in many other polarized cells, this depends on the activity of the Par complex (Goldstein & Macara 2007). As NBs enter prophase, the Par complex including Par3/Bazooka (Baz), aPKC and Par-6 assembles at the apical NB pole, which drives the localization of fate determinants to the basal NB pole (Wodarz et al. 1999; Wodarz et al. 2000; Rolls et al. 2003; Petronczki & Knoblich 2001; Betschinger et al. 2003; Choksi et al. 2006; Doe et al. 1991; Lu et al. 1998; Uemura et al. 1989; Knoblich et al. 1995; Homem & Knoblich 2012; Prehoda 2009; C.-Y. Lee et al. 2006; Bowman et al. 2008).

Upon self-renewing asymmetric NB division, the fate determinants segregate to the daughter cells, which will commit to differentiation. For this to happen correctly, two adapter proteins, Partner of Numb (Pon, (Lu et al. 1998)) and Miranda (Mira, (Ikeshima-Kataoka et al. 1997; Shen et al. 1997)), are

49 required. While Pon localizes the Notch signaling regulator Numb (Lu et al.
50 1998), Mira localizes the homeobox transcription factor Pros and the
51 translational repressor Brat to the basal NB cortex in mitosis (Ikeshima-
52 Kataoka et al. 1997) (Betschinger et al. 2006; C.-Y. Lee et al. 2006). In the
53 absence of Mira, fate determination is impaired and tumor-like growth can
54 occur in larval NB lineages (Ikeshima-Kataoka et al. 1997; Caussinus &
55 Gonzalez 2005).

56 How polarized Mira localization in mitotic NBs is achieved is a long-standing
57 question and despite being a well-studied process, this mechanism is not fully
58 understood. In embryonic NBs, Mira localization requires actin (Shen et al.
59 1998) and myosin activity since mutation in the myosin regulatory light chain
60 *spaghetti squash* (*sqh,* (Barros et al. 2003)) or the Myosin VI gene *jaguar*
61 (Petritsch et al. 2003) have been reported to lead to Mira localization defects.
62 Furthermore, in embryos injected with the Rho kinase (ROCK) inhibitor Y-
63 27632, Mira was uniformly localized to the cortex, which was rescued by the
64 expression of a phospho-mimetic *sqh* allele. This led to the proposal that
65 Myosin II plays a critical role in Mira localization and aPKC affects Mira
66 localization indirectly through regulating Myosin II (Barros et al. 2003).

67 However, it was then shown that Y-27632 can inhibit aPKC directly and that
68 Mira is a substrate of aPKC (Atwood & Prehoda 2009; Wirtz-Peitz et al. 2008).
69 In fact many aPKC substrates including Numb and Mira contain a basic and
70 hydrophobic (BH) motif that can be phosphorylated by aPKC. Upon
71 phosphorylation the substrates are no longer able to directly bind

phospholipids of the plasma membrane (PM) (Bailey & Prehoda 2015; Smith et al. 2007; Dong et al. 2015).

Asymmetric Mira localization in mitotic NBs can in principle be explained by keeping the activity of aPKC restricted to the apical pole (Atwood & Prehoda 2009). While this model offers a straightforward explanation for uniform Mira in *apkc* mutant NBs, it is less clear what the contribution of the actomyosin network to polarized Mira localization is. An untested possibility is that actomyosin acts as a stabilizing element for Mira basal localization in mitosis as suspected for aPKC substrates in other contexts (Bailey & Prehoda 2015).

Intriguingly, Mira localizes uniformly to the cortex of larval brain NBs in interphase (Sousa-Nunes et al. 2009) before becoming basally restricted in mitosis. In embryonic NBs, Mira and its cargo Pros localize to the apical cortex (Spana & Doe 1995) and Pros is found in the nucleus of interphase *mira* mutant NBs (Matsuzaki et al. 1998). Given that the levels of nuclear Pros in NBs is important for the regulation of entry and exit from quiescence and NB differentiation (Lai & Doe 2014), the regulation of cortical Mira in interphase might be important in this context. However, differences or similarities in the regulation and parameters of Mira binding in interphase and mitosis and the transition between the two different localizations have not yet been examined.

Using fluorescent reporters of the Par complex and Mira at endogenous levels of expression, we now reveal that cortical Mira localization is differently controlled in interphase, where it uniformly binds to the PM and after nuclear

envelope breakdown (NEB), when actomyosin activity is required. Therefore, by integrating the temporal order of events our results suggest that both phosphoregulation by aPKC and differential binding to the actin cortex are required for asymmetric Mira localization, but operate a different phases of the cell cycle.

RESULTS

Uniform Miranda is cleared from the cortex during prophase and Miranda reappears asymmetrically after NEB

We first confirmed in larval NBs that Mira localizes uniformly to the cortex in interphase (**Figure 1A**) and co-localizes with its cargo Pros in interphase and mitosis (**Figure 1 supplement 1**). We further stained *mira*^{L44} NBs for Mira and Pros. In these cells, Pros is predominantly found in the nucleus in interphase (**Figure 1 supplement 1**). These results suggest that Mira is required to keep Pros out of the NB nucleus throughout the cell cycle. We therefore sought to address the regulation of cortical Mira in interphase and mitosis and the transition between these localizations.

To accurately monitor *in vivo* the dynamics of this transition, we used a BAC construct in which Mira was tagged at its C-terminus with mCherry ((Ramat et al. 2017) and **Figure 1 supplement 2**). This tagged Mira recapitulated uniform cortical localization in interphase (**Figure 1B**, **-**33 to NEB) and polarized localization to the basal pole in mitosis (**Figure 1B**, +4), with a 2.5-fold increase in intensity (n=5, **Figure 1B'**).

This transition occurred in two distinct steps. Firstly, during prophase, after Mira was rapidly excluded from the apical pole where Baz started localizing (**Figure 1B,B' -**8 to NEB), Mira was progressively cleared from most of the rest of the cortex in an apical-to-basal direction (**Figure 1B,B'** -4 to NEB). Secondly, following NEB, Mira reappeared at the cortex in a basal crescent (**Figure 1B,B'** +4 after NEB). We further recapitulated these steps by antibody staining of endogenous, non-tagged Mira and using overexpression of GFP::Mira (**Figure 1 supplement 3**). Thus, Mira is first cleared form most of the cortex during prophase and only upon NEB reappears in a basal crescent (**Figure. 1C**). Furthermore, Baz and aPKC cortical dynamics were similar (related to **Movie S1** (Baz/Mira) and **Movie S2** (aPKC/Mira)).

Actomyosin is required for the establishment and maintenance of Miranda crescents after NEB

In embryonic NBs, Mira localization is sensitive to F-actin disruption in mitosis (Shen et al. 1998). We reasoned that this could be due to defective Mira clearance in prophase and/or defective Mira reappearance at the basal cortex after NEB. We tested this by disrupting the actin network of larval NBs with Latrunculin A (LatA). Despite efficiently disrupting F-actin (**Figure 2 supplement**) and causing cytokinesis failure (**Figure 2A,** 3:02, related to **Movie S3**), LatA treatment affected neither uniform cortical localization of Mira in interphase (**Figure 2A,** 2:06) nor its clearance during prophase (**Figure 2A,** 2:21). In contrast, Mira failed to relocalize to a basal crescent

following NEB in LatA-treated NBs (**Figure 2A,** 2:33). We next tested whether, in addition to crescent establishment, F-Actin controlled crescents maintenance. To this end, we arrested NBs with colcemid in metaphase (at which point Mira crescents are established), after which we treated them with LatA. Again, LatA caused Mira to relocalize to the cytoplasm (**Figure 2A**). Importantly, this relocalization is unlikely to be due to Mira being "swept off" the cortex by aPKC, which like Baz redistributes from an apical crescent to the entire cortex following LatA treatment (**Figure 2 supplement**). Unlike the gradual apical-to-basal clearance of Mira during prophase (**Figure 1B**), basal Mira crescents fall off the cortex homogenously upon LatA treatment. Furthermore, Mira falls off the cortex 2.8±1min (n=13) before aPKC becomes detectable basally (**Movie S4, Figure 2 supplement**). Therefore, an intact actin network is required to establish and maintain asymmetric Mira localization in mitotic larval NBs.

Myosin activity has been proposed to be required for Mira localization (Petritsch et al. 2003; Barros et al. 2003). We tested next which step of Mira localization involved Myosin. Myosin motor activity relies on the phosphoregulation regulatory light chain, encoded by the *sqh* gene in *Drosophila* (Jordan & Karess 1997), which we disrupted by applying ML-7, a specific inhibitor of the myosin light chain kinase (MLCK, (Bain et al. 2003)). As with LatA, the ML-7 treatment in cycling neuroblasts affected neither uniform cortical localization of Mira in interphase (**Figure 2B,** 0') nor its clearance during prophase (**Figure 2B,** 138-278') but resulted in failure to

167 establish a basal crescent after NEB, which was restored upon drug washout
168 (**Figure 2B**, 328'). In colcemid-arrested NBs, the ML-7 treatment also
169 resulted in Mira redistributing from the basal crescent to the cytoplasm, which
170 was restored upon ML-7 washout. Furthermore, unlike LatA treatment, ML-7
171 did not cause the Par complex to redistribute to the entire cortex (**Figure 2C,**
172 **Movie S5**). Finally, as in (Das & Storey 2014), we demonstrated the
173 specificity of the effect of ML-7 by counteracting its effect with a
174 phosphomimetic version of Myosin regulatory light chain: the overexpression
175 of a phosphomimetic version of Sqh (Sqh^{EE}, (Winter et al. 2001) significantly
176 delayed loss of cortical Mira after ML-7 addition in colcemid arrested NBs
177 (**Figure 2D, Movie S6**).
178 In conclusion, the contribution of F-Actin (Shen et al. 1998) and Myosin
179 (Petritsch et al. 2003; Barros et al. 2003) to asymmetric Mira localization is
180 linked to the relocalization of Mira and its maintenance at the basal cortex
181 following NEB, but not to the control of uniform cortical localization in
182 interphase or to clearance of Mira during prophase.
183
184 **Defective clearance of interphase cortical Miranda by aPKC results in**
185 **the persistence of uniform Miranda in mitosis.**
186 NBs mutant for aPKC also fail to asymmetrically localize Mira in mitosis (Rolls
187 et al. 2003), prompting us to investigate which aspect of Mira localization
188 involved aPKC in larval NBs. Like in controls, Mira localized uniformly to the
189 cortex of *apkc*^{k06403} (Wodarz et al. 2000) mutant NBs in interphase. However,
190 it did not clear from the cortex during prophase and instead remained

uniformly localized throughout mitosis (**Movie S7**, **Figure 3A**). Additionally, expressing a constitutively active form of aPKC, aPKC$^{\Delta N}$, resulted in the loss of uniform cortical Mira binding in interphase (**Figure 3 supplement**). These results show that during prophase, aPKC negatively regulates the uniform cortical localization of Mira observed in interphase. They also suggest that the failure to asymmetrically localize Mira in mitosis in aPKC mutants is due to defective clearance in prophase resulting in the abnormal persistence of uniform cortical Mira throughout mitosis.

We reasoned that, if this were the case, Mira localization in interphase should have the same characteristics as Mira localization in metaphase upon loss of function of aPKC. Consistent with this view, unlike Mira localization in mitosis, but similar to Mira localization in interphase (**Figure 2A**), Mira localization to the cortex in mitosis was insensitive to LatA treatment in NBs depleted for aPKC (**Figure 3 supplement**). To corroborate these results we used fluorescence redistribution after photo-bleaching (FRAP) to analyze the lateral diffusion/cytoplasmic exchange dynamics of Mira (**Figure 3B**). In controls, Mira redistributed about three times faster in interphase compared to mitosis (**Figure 3C, C'**), suggesting that Mira dynamics are indeed a relevant characteristic to analyze cell cycle-dependent control of Mira localization. Yet, in apparent contradiction with our proposition, aPKC impairment did not result in Mira redistribution in mitosis becoming as fast as in interphase. Instead, in NBs depleted for aPKC or expressing Lgl^{3A}, known to inhibit aPKC

(Betschinger et al. 2003), while Mira recovery became faster than in control mitosis, it did not become as fast as in control interphase (**Figure 3C, C'**). However, changes in the actin network caused by progression through the cell cycle (Ramanathan et al. 2015) can influence dynamics of membrane-associated proteins in general (Heinemann et al. 2013). This is also the case in NBs, as a photo-convertible membrane-associated reporter that attaches to the entire NB PM via a myristoylation signal (myr-Eos) showed similar slowing of dynamics in mitosis compared to interphase (~four-fold, **Figure 3D, CD'**). Thus, this general cell cycle-driven change of dynamics may account for the difference between Mira redistribution in interphase and in mitosis in aPKC-impaired NBs. We tested this by cancelling this general change by treating mitotic NBs with LatA, which resulted as expected in myr-Eos dynamics falling into ranges similar to interphase (**Figure 3D, D'**) and, in aPKC-impaired NBs, resulted in Mira redistribution rates getting as fast as in interphase (**Figure 3C, C'**). Importantly, myr-Eos dynamics were not sensitive to Lgl^{3A} overexpression alone, arguing against the possibility that aPKC impairment causes general changes in the cortex that could explain accelerated redistribution of Mira in this condition.

In conclusion, instead of being cleared, Mira persists throughout mitosis with the same actin-insensitive uniform localization and the same dynamics as in interphase in *apkc* mutant NBs.

238 **Miranda binds uniformly to the plasma membrane in interphase**

239 In *Drosophila* S2 cells Mira binds directly to phospholipids of the PM via its BH
240 motif and the ability to bind the PM is abolished upon phosphorylation of this
241 motif by aPKC (Bailey & Prehoda, 2015). Our results, that Mira cortical
242 localization in interphase is actin-independent and that its clearance in
243 prophase is aPKC dependent, suggest that that in interphase Mira is retained
244 uniformly at the PM by its BH motif.

245 Five aPKC phosphorylation sites have been identified in Mira, only one of
246 which (S96) directly resides in the BH motif (Bailey & Prehoda 2015). To
247 investigate its influence on dynamic Mira localization in neuroblasts, we used
248 CrispR to generate mCherry-tagged control Mira (S96, ctrl), a phosphomutant
249 version (S96A), a phosphomimetic version (S96D) - shown *in vitro* to reduce
250 phospholipid binding and Mira recruitment to the PM when overexpressed in
251 S2 cells (Bailey & Prehoda 2015) - and a complete deletion of the BH motif
252 (ΔBH, **Figure 4A**).

253 Control Mira localized uniformly to the cortex in interphase, was cleared from
254 the cortex in prophase and reappeared as a basal crescent after NEB (**Figure**
255 **4A, Movie S8**). In contrast, although phosphomutant Mira^{S96A} localized
256 uniformly to the cortex in interphase, it was not cleared in prophase and
257 failed to localize asymmetrically following NEB (**Figure 4A**, **Movie S9**),
258 consistent with our hypothesis that aPKC-dependent Mira clearance is caused
259 by the phosphorylation of its BH motif. Unexpectedly, Mira^{S96A} also presented
260 a transient apical enrichment during prophase, perhaps explainable by
261 abnormally stable interactions with apically localized aPKC, caused by the

inability of aPKC to phosphorylate Mira^{S96A}. Nonetheless, our hypothesis is further supported by the dynamics of phosphomimetic Mira^{S96D}, which were the mirror image of Mira^{S96A}: Mira^{S96D} did not localize to the cortex in interphase (and instead accumulated predominantly on cortical microtubules, as evidenced by its relocalization to the cytoplasm upon colcemid treatment (**Figure 4B**), and localized asymmetrically at the cortex following NEB (**Figure 4A**, **Movie S10**). Finally, deletion of the BH motif abolished both uniform cortical localization in interphase and asymmetric cortical localization after NEB (**Figure 4A**, **Movie S11,** see **Figure 4C** for quantification and **Figure 4D** for summary of the main localization of the different Mira mutants).

Therefore, our findings are consistent with Mira being bound via its BH motif to the phospholipids of the PM in interphase, and that phosphorylation of this motif by aPKC in prophase disrupts this interaction as observed in *Drosophila* S2 cells (Bailey & Prehoda, 2015).

Mira crescent size is affected by a Y-27632-sensitive mechanism that operates before NEB

So far, our results demonstrate that Mira binds the PM uniformly in interphase, is cleared from there by aPKC at the onset of prophase, but requires actomyosin upon NEB. This raises the question whether aPKC contributes to Mira asymmetric localization after NEB.

Temporal inactivation can be achieved with temperature sensitive (ts) alleles or small molecule inhibition. We find that the available ts allele of aPKC

(Guilgur et al. 2012) is hypomorphic already at permissive temperature resulting in Mira localization defects (not shown). Therefore, we made use of the non-specific effects of the ROCK inhibitor Y-27632, which inhibits aPKC with an IC50 of 10µM (Atwood & Prehoda 2009). When we added 50µM of Y-27632 to already polarized NBs, after 1h in the presence of the drug, we did not detect any significant changes in Mira or aPKC crescent size (n=22, **Figure 5A,** and **Figure 5 supplement**).

In striking contrast, when we added half that dose to cycling NBs, while aPKC crescent size was comparable to controls (**Fig 5 supplement**) Mira crescents formed, but were significantly enlarged. As a consequence daughter cell size was also increased (n=12, **Figure 5B, C**). Intriguingly, such enlarged crescents were LatA and ML-7 sensitive (**Figure 5D**), both indicators that enlarged Mira crescents were not due lack of phosphorylation of Mira by aPKC (**Figure 3** and **Figure 3 supplement**). However, when we titrated the Y-27632 concentration to induce uniform cortical Mira when added to cycling NBs, Mira became uniformly cortical and was insensitive to LatA treatment, suggesting that 200µM Y-27632 can lead to inhibition of Mira phosphorylation by aPKC at elevated concentrations (**Movie S12**, n=25).

We therefore treated colcemid arrested NBs with 200µM Y-27632. Surprisingly, it took 52±11min (n=15) until faint Mira signal became on average detectable apically, nevertheless Mira distribution remained always biased towards the basal pole in the presence of Y-27632. However, this

asymmetry was lost when we additionally added LatA after ~60min in Y-27632, which caused Mira to become uniformly distributed on the membrane (**Figure 5E**, **Movie 13**, n=15).

We conclude that Y-27632 at 200µM can inhibit aPKC's ability to phosphorylate Mira. At lower concentrations (25µM) Y-27632 also has an effect on Mira crescent size, but only before NEB, revealing a Y-27632-sensitive step that is unlikely to reflect aPKC inhibition. Furthermore, aPKC might contribute to Mira asymmetry after NEB by excluding Mira from the apical cortex, but a LatA sensitive biased distribution of Mira remains.

Discussion

In this study, we reinvestigated *in vivo* the precise contributions of aPKC and actomyosin to the asymmetric localization of the cell fate determinant adapter Mira. Using live cell imaging of *Drosophila* larval neuroblasts and fluorescent reporters at endogenous levels of expression, we reveal that aPKC and actomyosin contribute differently to Mira localization, at two different steps of mitosis. Live imaging was critical to this finding, as it allowed us to precisely describe the transition from the uniform localization of Mira at the cortex in interphase and its asymmetric localization in mitosis. We observed that it occurred in two steps: first, Mira was cleared from most of the cortex during prophase; second, Mira came back to the cortex as a basal crescent following

NEB. We then proceeded to assess the relative contributions of aPKC and actomyosin to these steps (**Figure 1**).

In interphase Mira binds uniformly to the NB plasma membrane. We engineered phosphomimetic and phosphomutant alleles of Mira to further show that, as described in *Drosophila* S2 cells (Bailey & Prehoda, 2015), aPKC-dependent clearance of Mira occurred through the phosphorylation of its BH motif. Importantly, the Mira^{S96A} phosphomutant, in which, among the five aPKC phosphorylation sites of Mira, only the one in the BH motif was affected, recapitulated the uniform localization (**Figure 4)** of a Mira phosphomutant of all five sites in neuroblasts in metaphase (Atwood & Prehoda 2009). The possible contribution of the four sites outside the BH motif remains to be investigated. Interestingly, deletion of the entire BH motif resulted in microtubule association of Mira in interphase. In addition to binding to phospholipids, Mira has been shown to be able to bind to microtubules (Chang et al. 2011) and we propose that Mira is simply sequestered at the PM in interphase, and when interfering with the ability to interact with one binding partner this might result in higher of Mira for another.

The transition from uniform PM binding to asymmetric basal localization is triggered from prophase, where aPKC activity removes Mira's ability to bind the PM uniformly (**Figure1, 4**). NEB appears to be a critical time point for basal crescent formation (**Figure 1**), which is in line with the recent finding

that factors released from the nucleus upon NEB are involved in regulating Mira localization (Zhang et al. 2016).

After NEB we find that actomyosin is important to retain Mira asymmetrically at the cortex (**Figure 2A-C**). This localization also requires the BH motif, but it is less sensitive to the S96D mutation, which retains the ability to asymmetrically bind the cortex (**Figure 4A**). It is possible that basal Mira localization occurs step-wise and maintenance requires accessory factors. Actomyosin is one of them and we found recently that maintenance of Mira asymmetry in mitotic NBs requires interaction of Mira and cognate mRNA (Ramat et al. 2017). Therefore, BH motif might be required to initiate basal Mira localization, allowing cytoplasmic Mira to interact with the PM also in mitosis, triggering its stabilization at the basal pole through accessory interactions.

Barros et al. (2003) suggested that myosin II is required to exclude Mira from the apical pole and push it into daughter cells during division. Our results rather suggest that myosin activity might be required to anchor Mira basally (**Figure 2C**). ML-7 and Y-27632 are thought to affect myosin activity through altering myosin light chain phosphorylation. However, the effects of the drugs on Mira differ. ML-7 affects anchoring of Mira to the basal cortex (**Figure 2C**), while Y-27632 affects Mira crescent size (**Figure 5B-D**). This could be the result of a combinatorial effect of Y-27632 on aPKC and Rho kinase, masking loss of anchoring. Furthermore, in MCDK II cells, Y-27632 and ML-7

381 treatment caused different effects on Myosin light chain phosphorylation
382 (Watanabe et al. 2007), potentially having different effects on myosin activity.
383 Furthermore, aPKC might be required after NEB to exclude Mira from the
384 apical pole (**Figure 5E**). However, at 200µM Y-27632, other processes might
385 be inhibited as well. Finally, we find that a Y-27632 sensitive step regulating
386 Mira crescent size. Then enlarged crescents do not appear to be caused by
387 lack of phosphorylation of Mira by aPKC (**Figure 5A-D**), suggesting that Rho
388 kinase could be involved in regulating Mira crescent size.
389
390 Why two different mechanisms to control Mira cortical binding? It might be
391 beneficial for the NB to tether Mira at the interphase cortex to sequester Pros,
392 which did not segregate during division and that might otherwise enter the
393 nucleus. In this way NBs could be protected from excess levels of fate
394 determinants, which can drive NBs out of the cell cycle (Choksi et al. 2006).
395 Nuclear Pros levels are also developmentally controlled, which has been
396 linked to the regulation of quiescence and NB differentiation (Lai & Doe
397 2014).
398
399 In larval NBs the regulation of nuclear Pros involves Hedgehog signaling and
400 the transcription factor *grainy head* (Chai et al. 2013; Maurange et al. 2008).
401 However, the cell biology underpinning this signaling is not clear. RanGEF BJ1
402 promotes Pros nuclear exclusion (Joy et al. 2014), but it is not clear whether
403 this is a direct effect. The ability to differentially regulate Mira localization
404 might be important in this context. Being able to regulate Mira's interaction

405 with the PM and at the actomyosin cortex might allow the system to release
406 the fate determinants in a controllable manner in the GMC while being able to
407 tune cortical/nuclear Pros levels through regulation of uniform Mira
408 localization to the plasma membrane in interphase.

409

410

411 **Materials & Methods**

412 *Fly stocks and genetics*

413 Flies were reared on standard corn meal food at 25 degrees. Lines used:
414 (1) Baz::GFP trap (Buszczak et al. 2007); (2) w^{1118} (Bloomington); (3)
415 MARCM: hsFlp tubGal4 UASnlsGFP; FRT42B tubGal80/Cyo and FRT82B gal80
416 (T. Lee & Luo 1999); (4) worniu-Gal4 (Albertson et al. 2004); (5) UAS-
417 Lgl^{3A}::GFP (Wirtz-Peitz et al. 2008); (6) UAS-Lgl^{3A} (Betschinger et al. 2003);
418 (7)*w1118, y,w, hsp70-flp; tubP-FRT>cd2>FRT-Gal4, UAS-GFP (Gift from* M.
419 Gho); (8) Mz1061 (Ito et al. 1995); (9) UAS-GFP::Mira (Mollinari et al. 2002).
420 (10) FRT82B $mira^{L44}$ (Matsuzaki et al. 1998). (10) Df(3R)ora^{I9} (Shen et al.
421 1997). (11) UAS-$aPKC^{RNAi}$: *P{y[+t7.7] v[+t1.8]=TRiP.HMS01320}attP2*
422 (BL#34332)*; (12)* Numb::GFP (Couturier et al. 2013); (13) FRT42B $apkc^{k06403}$
423 (Wodarz et al. 2000)*;* (14) UAS-$aPKC^{\Delta N}$; (15) P{UASp-sqh.E20E21}3
424 (BL#64411); (16) P{10xUAS-IVS-mye::tdEos]attP2 (BL #32226); y[1] w[*];
425 P{y[+t*] w[+mC]=UAS-Lifeact-Ruby}VIE-19A (BL# 35545); (17) aPKC::GFP
426 (Besson et al. 2015); *Source 1 of Mira::mCherry: BAC{mira::mcherry-MS2}*
427 (Ramat et al. 2017). $aPKC^{RNAi}$ clones were generated by heat-shocking larvae
428 of the genotype *y,w, hsp70-flp; tubP-FRT>cd2>FRT-Gal4, UAS-GFP;*
429 *P{y[+t7.7] v[+t1.8]=TRiP.HMS01320}attP2*. Heat shocks were performed
430 24hph and 48hph for 1 hour at 37ºC. MARCM clones were generated by heat
431 shocking L1 larvae for 2h at 37°C.
432 Generation of Mira alleles: Source 2 of Mira::mCherry: $mira^{mCherry}$;
433 $mira^{\Delta BHmCherry}$ (Ramat et al. 2017), $mira^{S96A\text{-}mCherry}$ and $mira^{S96D\text{-}mCherry}$ are
434 derived from $mira^{KO}$ (Ramat et al. 2017). $mira^{mCherry}$ was generated by

435 inserting a modified wt genomic locus in which mCherry was fused to the C-
436 terminus following a GSAGS linker into *mira*^{KO}. For *mira*$^{S96D\text{-}mCherry}$: TCG
437 (Serine96) was changed to GAC (aspartic acid). For *mira*$^{S96A\text{-}mCherry}$: TCG was
438 replaced with GCG (alanine). CH322-11-P04 was the source for the *mira*
439 sequences cloned using Gibson assembly into the RIV white vector (Baena-
440 Lopez et al. 2013) that was injected using the attP site in *mira*^{KO} as landing
441 site. *mira*^{BACmCherry} (Ramat et al. 2017) (**see Figure 1 supplement 2**). While
442 mira^{mCherry} behaves similarily to *mira*^{BACmCherry} and rescues embryonic lethality,
443 mira$^{\Delta BHmCherry}$, mira$^{S96A\text{-}mCherry}$ and mira$^{S96D\text{-}mCherry}$ are homozygous lethal.
444
445 Live imaging: Live imaging was performed as described (Pampalona et al.
446 2015). Briefly, brains were dissected in collagenase buffer and incubated in
447 collagenase for 20 minutes. Brains were transferred to a drop of fibrinogen
448 (0.2mgml^{-}1, Sigma f-3879) dissolved in Schneider's medium (SLS-04-351Q)
449 on a 25mm Glass bottom dish (WPI). Brains were manually dissociated with
450 needles before the fibrinogen was clotted by addition of thrombin (100Uml^{-1},
451 Sigma T7513). Schneider's medium supplemented with FCS, Fly serum and
452 Insulin was then added. A 3-4µm slice at the centre of the neuroblasts was
453 then imaged every 30-90s using a 100x OIL objective NA1.45 on a spinning
454 disk confocal microscope. Data was processed and analyzed using FIJI
455 (Schindelin et al. 2012). For nuclear volume measurements Imaris was used.
456 All other drugs were added to the media either prior or during imaging: ML-7
457 (Sigma, I2764, dissolved in water), Y-27632 (Abcam, Ab120129, dissolved in
458 water). Drugs were washed out by media replacement, in the polarity
459 reconstitution assay colcemid concentrations were kept constant throughout
460 the experiments. FRAP experiments were carried out on a Leica SP8 confocal
461 using a 63x NA1.2 APO water immersion objective. To estimate $t_{1/2}$ for the
462 recovery curves we used published curve fitting methods (Rapsomaniki et al.
463 2012).
464
465
466

Immunohistochemistry

Primary cell culture: Brains were dissected in collagenase buffer and incubated for 20 minutes in collagenase, as for live imaging. Brains were then transferred into supplemented Schneider's medium and manually dissociated by pipetting up and down. Cells were pipetted onto a poly-lysine coated 25mm glass bottomed dish and left to adhere for 40 minutes. Schneider's was then replaced with 4% Formaldehyde (Sigma) in PBS and cells were fixed for 10 minutes. Cells were permeabilized with 0.1% PBS-Triton for 10 minutes. Cells were then washed with PBS 3x 10minutes before antibody staining overnight at 4ºC. All antibodies were dissolved in PBS-1%Tween. *Whole mount brains*: Brains were fixed in 4% Formaldehyde (Sigma) for 20 minutes at room temperature. Primary antibodies: Rabbit anti-Miranda (1:200, gift from C. Gonzalez), Mouse anti-GFP (1:400, Abcam). Rabbit anti-Brat (1:200, a gift from J. Knoblich). Guinea Pig anti-Dpn (1:500 a gift from J. Skeath). Mouse anti-Pros (1:40, DSHB). To stain F-Actin we used Alexa Fluor 488 or 561 coupled Phalloidin (Molecular Probes, 5:200) for 20 minutes at room temperature. Secondary antibodies (all from life technologies and raised in donkey: Anti-Rabbit Alexa-594, Anti-Mouse Alexa-488, Anti-Rabbit Alexa-647, Anti-Guinea Pig Alexa-647. Microscopy was performed using a Leica-SP8 CLSM (60x Water objective, 1.2) and images were processed using FIJI.

In all cases the sample size *n* provided reflects all samples collected for one experimental condition. Experimental conditions were repeated at least twice to account for technical and biological variation.

Acknowledgements

We thank C. Doe, J. Knoblich, F. Schweisguth, D. StJohnston, F. Matsuzaki, C. Gonzalez, J. Skeath, A. Wodarz, M. Gho and the Kyoto and Bloomington stock centers for reagents and/or protocols. We thank A. Müller, C. Weijer and M. Gonzalez-Gaitan for critical reading. M.R.H is supported by an MRC PhD studentship. We thank inDroso (http://www.indroso.com) for the generation of *mira*^{attPko} by CrispR and the Dundee imaging facility for excellent support.

Work in J.J.'s laboratory is supported by Wellcome and the Royal Society Sir Henry Dale fellowship 100031Z/12/Z. The tissue imaging facility is supported by the grant WT101468 from Wellcome.

References

Albertson, R. et al., 2004. Scribble protein domain mapping reveals a multistep localization mechanism and domains necessary for establishing cortical polarity. *Journal of Cell Science*, 117(Pt 25), pp.6061–6070.

Alexandre, P. et al., 2010. Neurons derive from the more apical daughter in asymmetric divisions in the zebrafish neural tube. *Nature Neuroscience*, 13(6), pp.673–679.

Atwood, S.X. & Prehoda, K.E., 2009. aPKC phosphorylates Miranda to polarize fate determinants during neuroblast asymmetric cell division. *Current biology : CB*, 19(9), pp.723–729.

Baena-Lopez, L.A. et al., 2013. Accelerated homologous recombination and subsequent genome modification in Drosophila. *Development*.

Bailey, M.J. & Prehoda, K.E., 2015. Establishment of Par-Polarized Cortical Domains via Phosphoregulated Membrane Motifs. *Developmental Cell*, 35(2), pp.199–210.

Bain, J. et al., 2003. The specificities of protein kinase inhibitors: an update. *The Biochemical journal*, 371(Pt 1), pp.199–204.

Barros, C.S., Phelps, C.B. & Brand, A.H., 2003. Drosophila nonmuscle myosin II promotes the asymmetric segregation of cell fate determinants by cortical exclusion rather than active transport. *Developmental Cell*, 5(6), pp.829–840.

Besson, C. et al., 2015. Planar Cell Polarity Breaks the Symmetry of PAR Protein Distribution prior to Mitosis in Drosophila Sensory Organ Precursor Cells. *Current biology : CB*, 25(8), pp.1104–1110.

Betschinger, J., Mechtler, K. & Knoblich, J.A., 2006. Asymmetric segregation of the tumor suppressor brat regulates self-renewal in Drosophila neural stem cells. *Cell*, 124(6), pp.1241–1253.

Betschinger, J., Mechtler, K. & Knoblich, J.A., 2003. The Par complex directs asymmetric cell division by phosphorylating the cytoskeletal protein Lgl. *Nature Cell Biology*, 422(6929), pp.326–330.

Bowman, S.K. et al., 2008. The tumor suppressors Brat and Numb regulate transit-amplifying neuroblast lineages in Drosophila. *Developmental Cell*, 14(4), pp.535–546.

Buszczak, M. et al., 2007. The carnegie protein trap library: a versatile tool for Drosophila developmental studies. *Genetics*, 175(3), pp.1505–1531.

Caussinus, E. & Gonzalez, C., 2005. Induction of tumor growth by altered stem-cell asymmetric division in Drosophila melanogaster. *Nature Genetics*, 37(10), pp.1125–1129.

Chai, P.C. et al., 2013. Hedgehog signaling acts with the temporal cascade to promote neuroblast cell cycle exit., 11(2), p.e1001494.

539 Chang, C.-W. et al., 2011. Anterior-posterior axis specification in Drosophila oocytes:
540 identification of novel bicoid and oskar mRNA localization factors. *Genetics*, 188(4),
541 pp.883–896.

542 Choksi, S.P. et al., 2006. Prospero acts as a binary switch between self-renewal and
543 differentiation in Drosophila neural stem cells. *Developmental Cell*, 11(6), pp.775–789.

544 Couturier, L., Mazouni, K. & Schweisguth, F., 2013. Numb localizes at endosomes and
545 controls the endosomal sorting of notch after asymmetric division in Drosophila. *Current*
546 *biology : CB*, 23(7), pp.588–593.

547 Doe, C.Q., 2008. Neural stem cells: balancing self-renewal with differentiation. *Development*,
548 135(9), pp.1575–1587.

549 Doe, C.Q. et al., 1991. The prospero gene specifies cell fates in the Drosophila central
550 nervous system. *Cell*, 65(3), pp.451–464.

551 Dong, W. et al., 2015. A conserved polybasic domain mediates plasma membrane targeting
552 of Lgl and its regulation by hypoxia. *The Journal of Cell Biology*, 211(2), pp.273–286.

553 Fuerstenberg, S. et al., 1998. Identification of Miranda protein domains regulating
554 asymmetric cortical localization, cargo binding, and cortical release. *Molecular and*
555 *cellular neurosciences*, 12(6), pp.325–339.

556 Goldstein, B. & Macara, I.G., 2007. The PAR proteins: fundamental players in animal cell
557 polarization. *Developmental Cell*, 13(5), pp.609–622.

558 Guilgur, L.G. et al., 2012. Drosophila aPKC is required for mitotic spindle orientation during
559 symmetric division of epithelial cells. *Development*, 139(3), pp.503–513.

560 Homem, C.C.F. & Knoblich, J.A., 2012. Drosophila neuroblasts: a model for stem cell biology.
561 *Development*, 139(23), pp.4297–4310.

562 Ikeshima-Kataoka, H. et al., 1997. Miranda directs Prospero to a daughter cell during
563 Drosophila asymmetric divisions. *Nature Cell Biology*, 390(6660), pp.625–629.

564 Ito, K., Urban, J. & Technau, G.M., 1995. Distribution, classification, and development
565 ofDrosophila glial cells in the late embryonic and early larval ventral nerve cord. *Roux's*
566 *archives of developmental biology*, 204(5), pp.284–307.

567 Jordan, P. & Karess, R., 1997. Myosin light chain-activating phosphorylation sites are required
568 for oogenesis in Drosophila. *Journal of Cell Biology*, 139(7), pp.1805–1819.

569 Joy, T., Hirono, K. & Doe, C.Q., 2014. The RanGEF Bj1 promotes prospero nuclear export and
570 neuroblast self-renewal. *Developmental neurobiology*, pp.n/a–n/a.

571 Knoblich, J.A., 2008. Mechanisms of asymmetric stem cell division. *Cell*, 132(4), pp.583–597.

572 Knoblich, J.A., Jan, L.Y. & Jan, Y.N., 1995. Asymmetric segregation of Numb and Prospero
573 during cell division. *Nature Cell Biology*, 377(6550), pp.624–627.

574 Kocsis, E. et al., 1991. Image averaging of flexible fibrous macromolecules: the clathrin
575 triskelion has an elastic proximal segment. *Journal of structural biology*, 107(1), pp.6–14.

576 Lai, S.-L. & Doe, C.Q., 2014. Transient nuclear Prospero induces neural progenitor
577 quiescence. *eLife*, 3.

578 Lee, C.-Y. et al., 2006. Brat is a Miranda cargo protein that promotes neuronal differentiation
579 and inhibits neuroblast self-renewal. *Developmental Cell*, 10(4), pp.441–449.

580 Lee, T. & Luo, L., 1999. Mosaic analysis with a repressible cell marker for studies of gene
581 function in neuronal morphogenesis. *Neuron*, 22(3), pp.451–461.

582 Lu, B. et al., 1998. Partner of Numb colocalizes with Numb during mitosis and directs Numb
583 asymmetric localization in Drosophila neural and muscle progenitors. *Cell*, 95(2), pp.225–
584 235.

585 Marthiens, V. & ffrench-Constant, C., 2009. Adherens junction domains are split by
586 asymmetric division of embryonic neural stem cells. *EMBO reports*, 10(5), pp.515–520.

587 Matsuzaki, F. et al., 1998. miranda localizes staufen and prospero asymmetrically in mitotic
588 neuroblasts and epithelial cells in early Drosophila embryogenesis. *Development*,
589 125(20), pp.4089–4098.

590 Maurange, C., Cheng, L. & Gould, A.P., 2008. Temporal transcription factors and their targets
591 schedule the end of neural proliferation in Drosophila. *Cell*, 133(5), pp.891–902.

592 Mollinari, C., Lange, B. & Gonzalez, C., 2002. Miranda, a protein involved in neuroblast
593 asymmetric division, is associated with embryonic centrosomes of Drosophila
594 melanogaster. *Biology of the cell / under the auspices of the European Cell Biology*
595 *Organization*, 94(1), pp.1–13.

596 Morais-de-Sá, E., Mirouse, V. & St Johnston, D., 2010. aPKC phosphorylation of Bazooka
597 defines the apical/lateral border in Drosophila epithelial cells. *Cell*, 141(3), pp.509–523.

598 Ohshiro, T. et al., 2000. Role of cortical tumour-suppressor proteins in asymmetric division of
599 Drosophila neuroblast. *Nature Cell Biology*, 408(6812), pp.593–596.

600 Pampalona, J. et al., 2015. Time-lapse recording of centrosomes and other organelles in
601 Drosophila neuroblasts. *Methods in cell biology*, 129, pp.301–315.

602 Petritsch, C. et al., 2003. The Drosophila myosin VI Jaguar is required for basal protein
603 targeting and correct spindle orientation in mitotic neuroblasts. *Developmental Cell*, 4(2),
604 pp.273–281.

605 Petronczki, M. & Knoblich, J.A., 2001. DmPAR-6 directs epithelial polarity and asymmetric cell
606 division of neuroblasts in Drosophila. *Nature Cell Biology*, 3(1), pp.43–49.

607 Prehoda, K.E., 2009. Polarization of Drosophila neuroblasts during asymmetric division. *Cold*
608 *Spring Harbor perspectives in biology*, 1(2), pp.a001388–a001388.

609 Ramat, A., Hannaford, M. & Januschke, J., 2017. Maintenance of Miranda localization in
610 Drosophila Neuroblasts involves interaction with the cognate mRNA. *Current Biology*, in
611 press.

612 Rapsomaniki, M.A. et al., 2012. easyFRAP: an interactive, easy-to-use tool for qualitative and
613 quantitative analysis of FRAP data. *Bioinformatics (Oxford, England)*, 28(13), pp.1800–
614 1801.

615 Rolls, M.M. et al., 2003. Drosophila aPKC regulates cell polarity and cell proliferation in
616 neuroblasts and epithelia. *Journal of Cell Biology*, 163(5), pp.1089–1098.

617 Schindelin, J. et al., 2012. Fiji: an open-source platform for biological-image analysis. *Nature*
618 *methods*, 9(7), pp.676–682.

Shen, C.P. et al., 1998. Miranda as a multidomain adapter linking apically localized Inscuteable and basally localized Staufen and Prospero during asymmetric cell division in Drosophila. *Genes & Development*, 12(12), pp.1837–1846.

Shen, C.P., Jan, L.Y. & Jan, Y.N., 1997. Miranda is required for the asymmetric localization of Prospero during mitosis in Drosophila. *Cell*, 90(3), pp.449–458.

Smith, C.A. et al., 2007. aPKC-mediated phosphorylation regulates asymmetric membrane localization of the cell fate determinant Numb. *The EMBO journal*, 26(2), pp.468–480.

Sousa-Nunes, R., Chia, W. & Somers, W.G., 2009. Protein phosphatase 4 mediates localization of the Miranda complex during Drosophila neuroblast asymmetric divisions. *Genes & Development*, 23(3), pp.359–372.

Spana, E.P. & Doe, C.Q., 1995. The prospero transcription factor is asymmetrically localized to the cell cortex during neuroblast mitosis in Drosophila. *Development*, 121(10), pp.3187–3195.

Uemura, T. et al., 1989. numb, a gene required in determination of cell fate during sensory organ formation in Drosophila embryos. *Cell*, 58(2), pp.349–360.

Watanabe, T., Hosoya, H. & Yonemura, S., 2007. Regulation of myosin II dynamics by phosphorylation and dephosphorylation of its light chain in epithelial cells. *Molecular biology of the cell*, 18(2), pp.605–616.

Winter, C.G. et al., 2001. Drosophila Rho-associated kinase (Drok) links Frizzled-mediated planar cell polarity signaling to the actin cytoskeleton. *Cell*, 105(1), pp.81–91.

Wirtz-Peitz, F., Nishimura, T. & Knoblich, J.A., 2008. Linking cell cycle to asymmetric division: Aurora-A phosphorylates the Par complex to regulate Numb localization. *Cell*, 135(1), pp.161–173.

Wodarz, A. et al., 1999. Bazooka provides an apical cue for Inscuteable localization in Drosophila neuroblasts. *Nature Cell Biology*, 402(6761), pp.544–547.

Wodarz, A. et al., 2000. Drosophila atypical protein kinase C associates with Bazooka and controls polarity of epithelia and neuroblasts. *Journal of Cell Biology*, 150(6), pp.1361–1374.

Zhang, F. et al., 2016. Phosphotyrosyl phosphatase activator facilitates localization of Miranda through dephosphorylation in dividing neuroblasts. *Development*, 143(1), pp.35–44.

Figures & Figure Legends

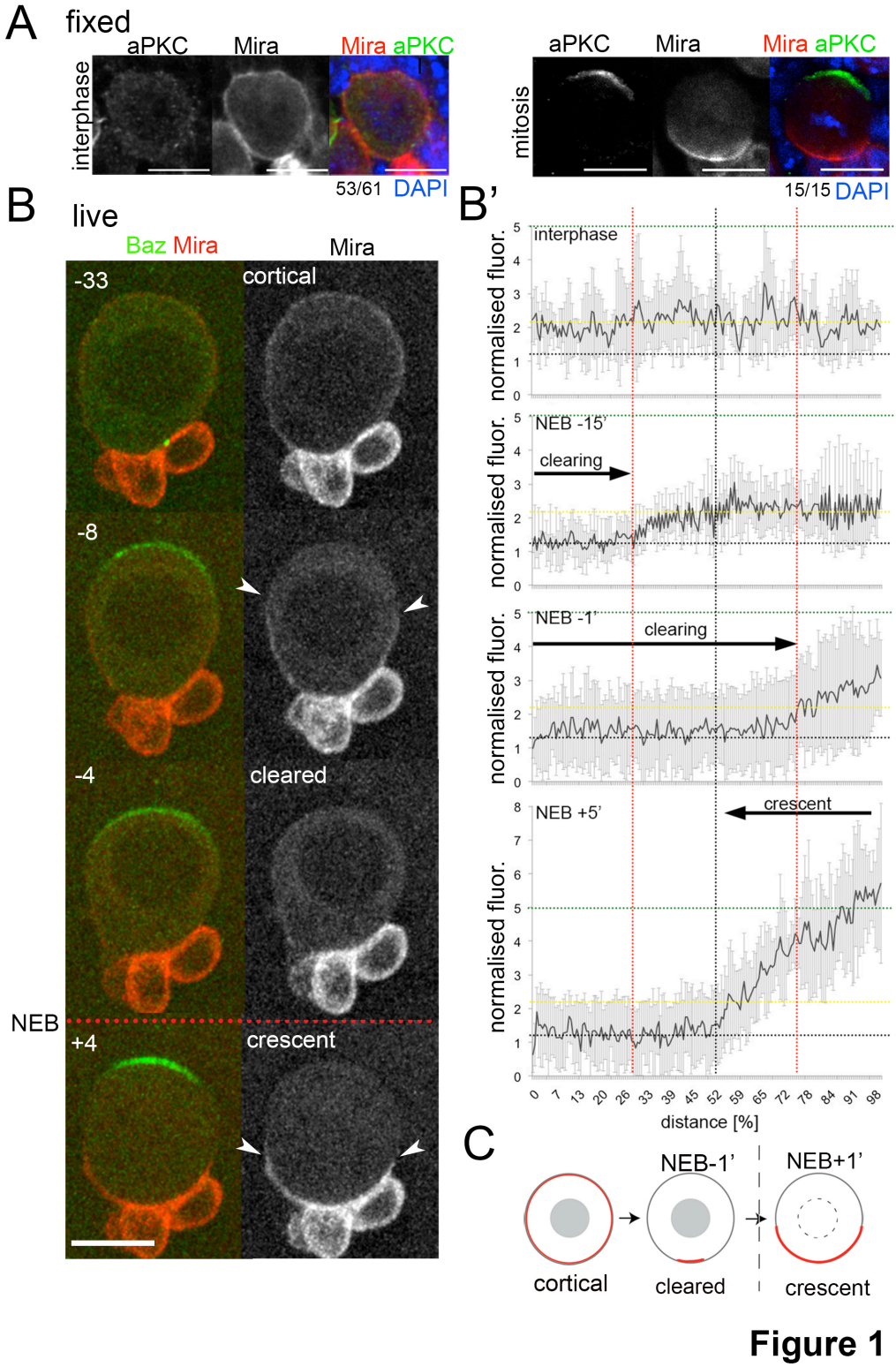

Figure 1

Figure 1. Miranda is cleared from the cortex before localizing in a basal crescent in mitosis. (**A**) Fixed larval brains showing NBs at the indicated cell cycle stage. (**B**) Selected frames from **Movie S1**. NB in primary cell culture expressing Baz::GFP (green) and Mira::mCherry (red) in the

transition from interphase to mitosis. Arrowheads point at Mira being cleared (-23) and at basal Mira crescent (+4). (**B'**) Quantification of cortical Mira::mCherry signal plotting the fluorescence intensities from the apical (center of GFP crescent at NEB) to the basal pole (center of mCherry signal at NEB) computationally straightening (Kocsis et al. 1991) the cortices of 5 NBs against the distance in % from the apical to the basal pole. Fluorescence was background subtracted and normalized to background subtracted cytoplasmic signal (1, dotted line). Cortical signal (yellow dotted line) and signal after NEB (green dotted line) Error bars, standard deviation. (**C**) Schematic representation of Mira localization at indicated time points in the cell cycle. *BAC{mira::mcherry-MS2}* was the source of Mira::mCherry. Scale bar 10µm. Time stamp: minutes.

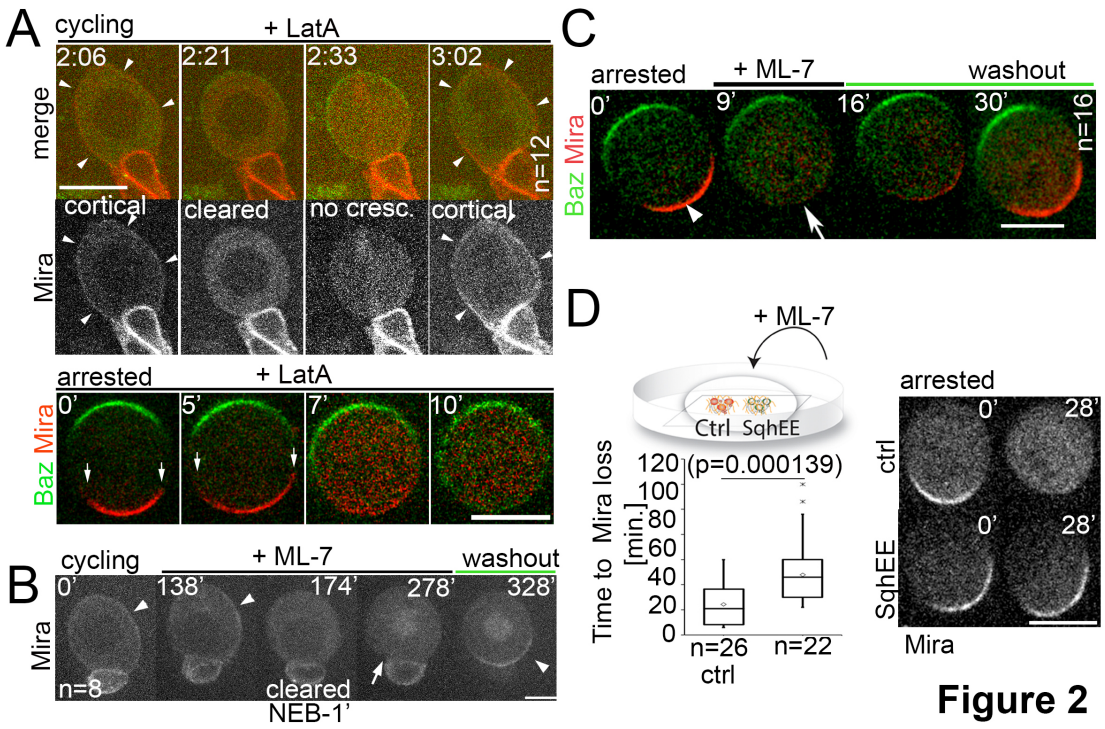

Figure 2

Figure 2. Differential response of Mira localization in interphase and mitosis to disruption of the actin network. (**A**) Stills from **Movie S3**. LatA was added to a cycling NB in primary cell culture expressing Baz::GFP (green) and Mira::mCherry (red). Arrowheads point at cortical Mira after culturing ~1h with LatA (2:06). At 1 min to NEB, Mira::mCherry is cleared from the cortex (2:21). Mira forms no crescent in the next mitosis (2:33), but after cytokinesis fails (note the bi-nucleated cell at 3:02, Baz panel), Mira is recruited to the cortex (arrowheads, 3:02). Bottom panels: Colcemid arrested NBs expressing Baz::GFP and Mira::mCherry. 5μM LatA was added prior to imaging at 15sec. intervals. Mira crescents (arrows) are lost upon LatA treatment. (**B**) Cycling NB in primary cell culture expressing Mira::mCherry, that remains cortical upon ML-7 addition (15μM; interphase: 0' and 138', arrowheads), is cleared 1minute prior to NEB (174'), does not form a crescent after NEB (arrow), but accumulates on the spindle (seen in cross section). After ML-7 washout, a basal Mira::mCherry crescent recovers (arrowhead, 328'). (**C**) Related to **Movie S5.** Colcemid arrested NB in primary cell culture expressing Baz::GFP (green) and Mira::mCherry (red). After addition of 20μM ML-7 Mira (arrowhead, 0') becomes cytoplasmic (arrow, +9'), but upon ML-7 washout a Mira crescent recovers. (**D**) The effect of 20μM ML-7 can be

quenched by overexpressing a phospho-mimetic form Sqh (Sqh^{EE}). Colcemid arrested NBs (ctrl: Mira::mCherry: SqhEE: Mira::mCherry co-expressing SqhEE by worniuGal4). Ctrl and SqhEE were co-cultured and ML-7 was added (related to **Movie S6**). Quantification of the time required to cause Mira::mCherry to become cytoplasmic shown on the left. Two-tailed ttest for independent means revealed significance. *BAC{mira::mcherry-MS2}* was the source of Mira::mCherry. Scale bar: 10µm.

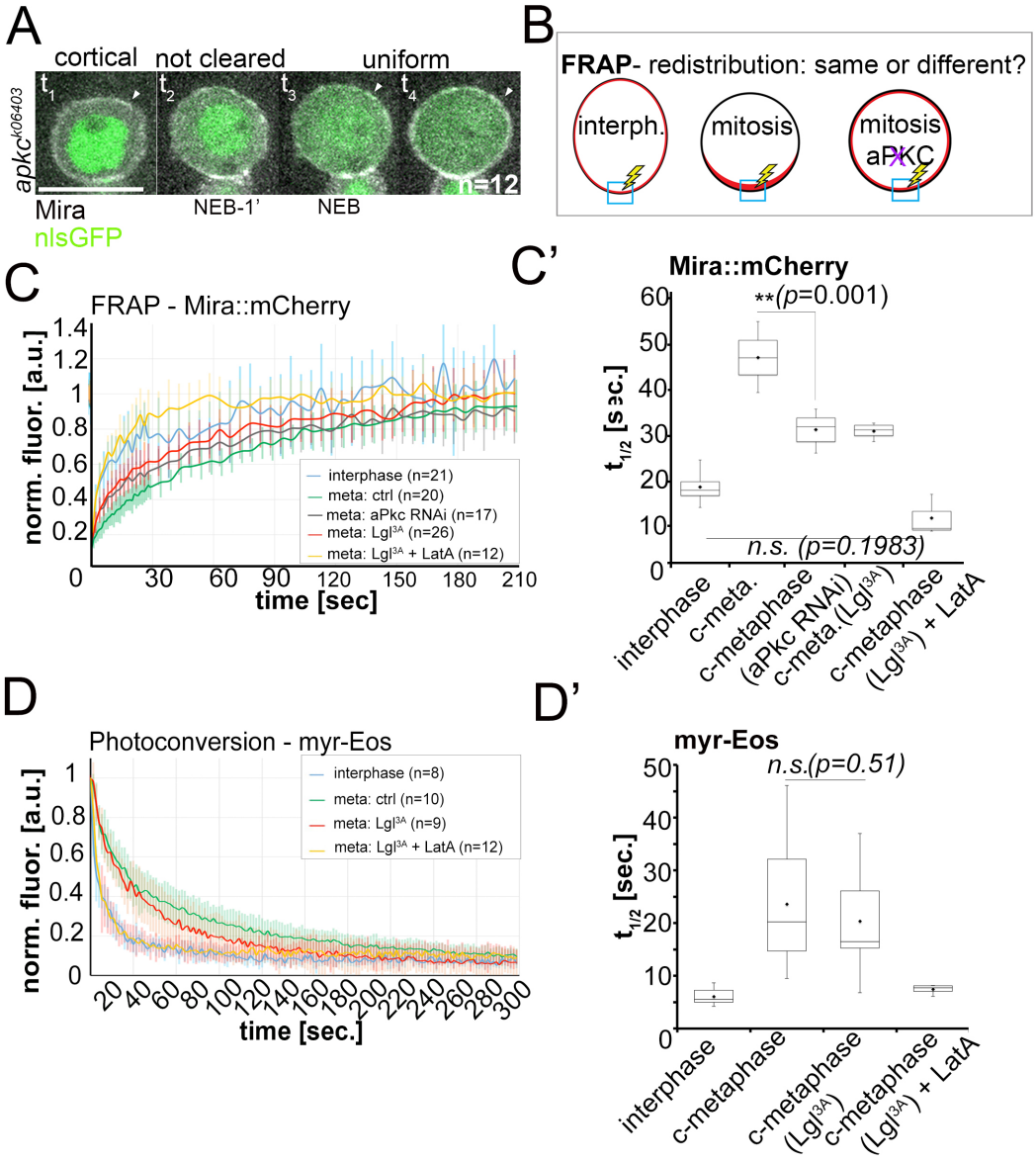

Figure 3

Figure 3. Lateral diffusion and cytoplasmic exchange of cortical Miranda are different in control and aPKC impaired mitotic NBs. (**A**) Stills from **Movie S7** of an *apkc*^{k06403} mutant NB (MARCM clone labeled with nlsGFP, green) expressing Mira::mCherry (grey). Mira is cortical in interphase, as the NB enters mitosis and after NEB (arrowheads, -20', -1, NEB, +5). (**B**) Conditions analyzed by FRAP. (**C**) Fluorescence redistribution curves of cortical Mira::mCherry at the indicated conditions. (**C'**) Estimates of $t_{1/2}$ [sec.] for cortical Mira::mCherry under the indicated conditions derived from curve fitting (Rapsomaniki et al. 2012). (**D**) Photo conversion experiment monitoring loss of myr-EOS converted signal over time. (**D'**) Estimates of $t_{1/2}$ [sec.] for cortical Mira::mCherry under the indicated conditions from curve fitting. Overexpression was driven by worniu-Gal4. p values: two-tailed ttest for independent means.

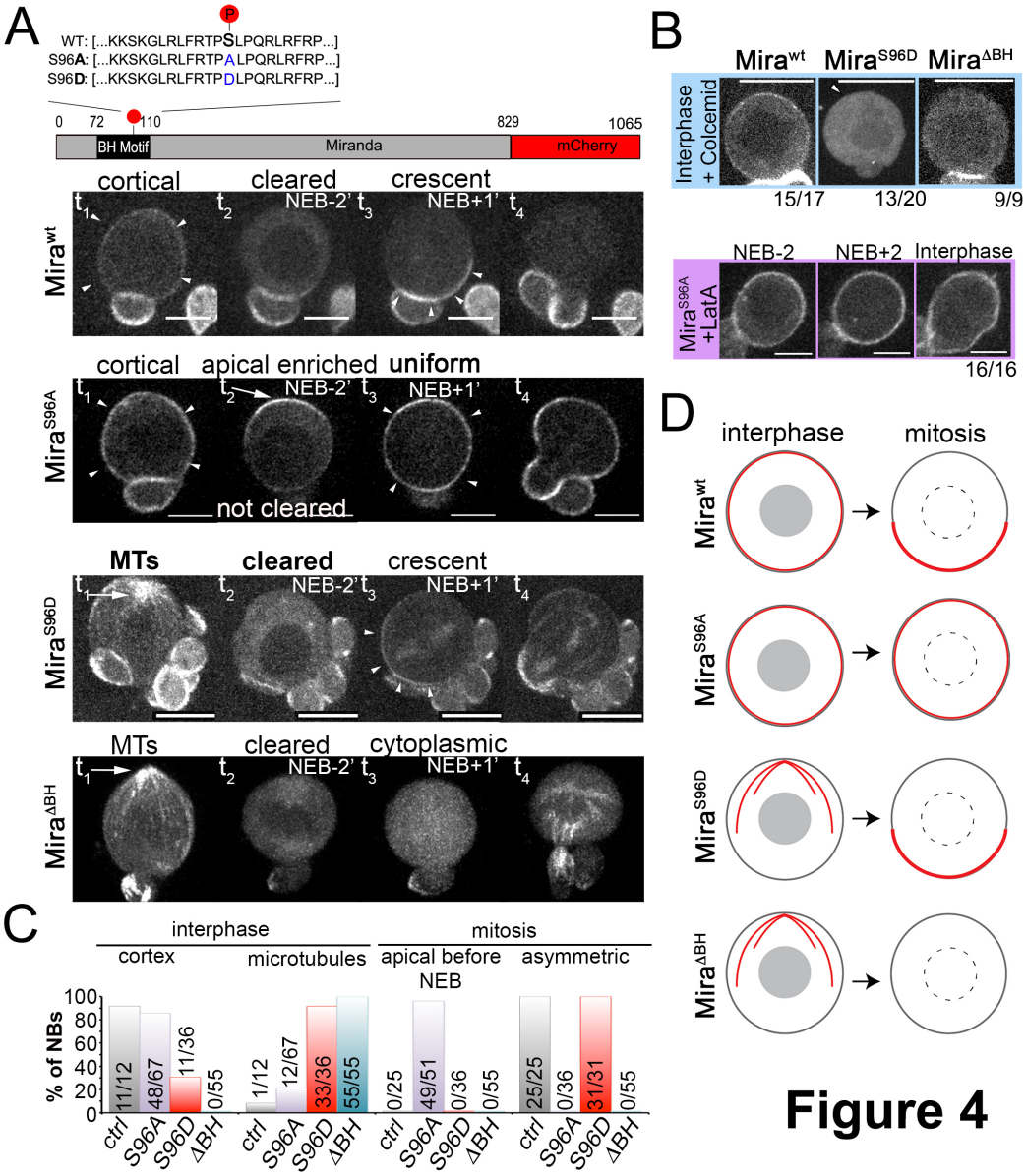

Figure 4

738

739 **Figure 4. Miranda binds to the plasma membrane in interphase NBs**
740 **via its BH motif** (**A**) Schematic indicating the different Mira alleles used.
741 CrispR generated Mira::mCherry localizes cortically uniform in interphase
742 (arrowheads t_1), is cleared from the cortex shortly before NEB and forms a
743 crescent (arrowheads t_3) thereafter that is inherited by daughter cells (related
744 to **Movie S8**). The phosphomutant S96A is uniformly cortical in interphase,
745 accumulates apically shortly before NEB, is uniformly cortical after NEB
746 (arrowheads t_3) and in division (related to **Movie S9**). The phosphomimetic
747 S96D localizes to cortical microtubules in interphase (arrow t_1), is cleared
748 from the cortex before NEB and asymmetric after NEB (arrowheads t_3) and
749 segregates to daughter cells (related to **Movie S10**). Deletion of the BH

motif leads to cortical microtubule localization in interphase (arrow t_1), cytoplasmic localization before and after NEB and reappearance on microtubules around cytokinesis (related to **Movie S11**). (**B**) Neuroblasts expressing the indicated Mira alleles were treated with 50µM colcemid for 60min. Control remains cortical, S96D and ΔBH become cytoplasmic. Cortical localization of S96A is further insensitive to LatA treatment. (**C**) Frequency of indicated localization of the different Mira alleles. (**D**) Schematic representation of the localization of the different Mira alleles. Scale bar:10µm.

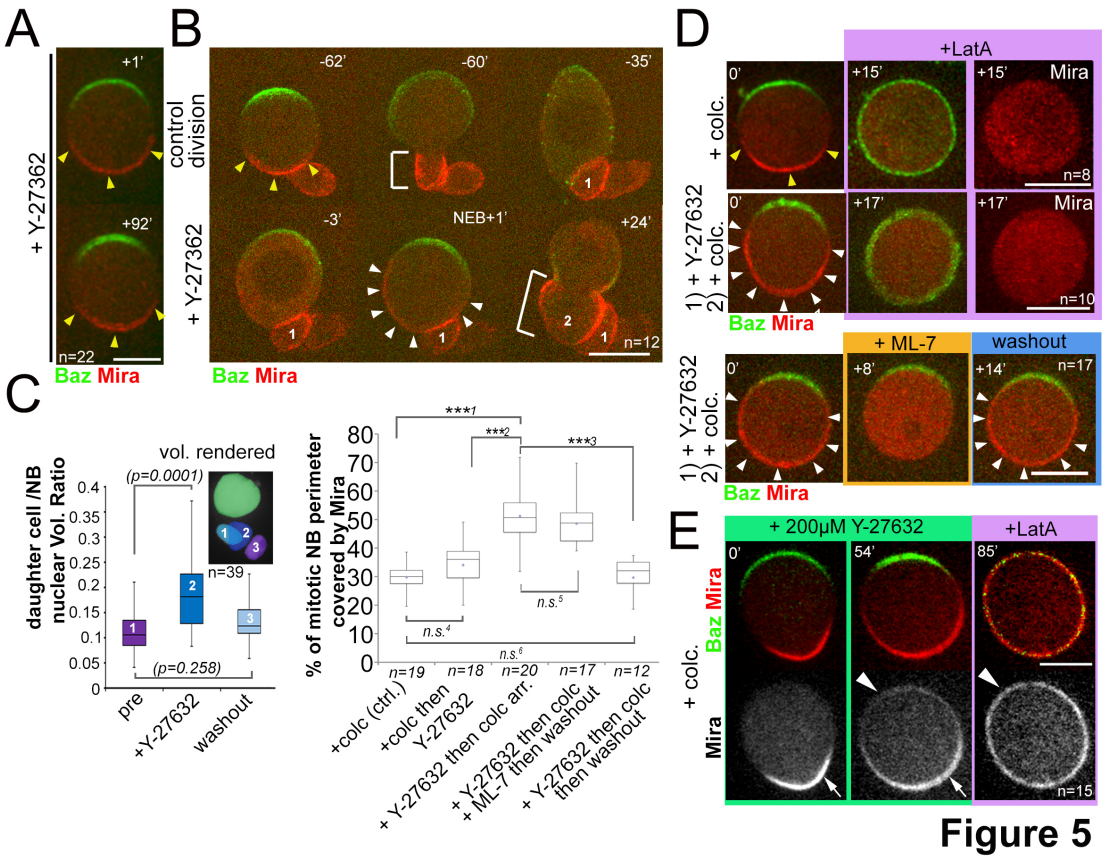

Figure 5

Figure 5. Mira crescent size is affected by a Y-27632-sensitive mechanism that operates before NEB. (**A**) Culturing colcemid arrested NBs in 50µM Y-27632 did not alter Mira crescent size (yellow arrowheads). (**B**) NBs polarizing in the presence of 25µM Y-27632 show enlarged Mira crescents. Control division (-62' to -35') with normally sized Mira crescent (bracket in -60', 1). Dividing in the presence of Y-27632 (-3, NEB+1) leads to an enlarged Mira crescent (NEB+1, white arrowheads) and enlarged daughter cell size (+24', brackets, 2). (**C**) Plot of the ratio of daughter cell to NB nuclei

as a measure for the effect of Y-27632 on daughter cell size. NBs expressing NLSGFP were imaged by DIC to follow daughter cell birth order during three consecutive divisions [1) pre-treatment; 2) div. in the presence of 25µM Y-27632; 3) div. after drug washout]. Then a high-resolution z-stack of nlsGFP was recorded, and the nuclear volumes rendered and calculated using IMARIS to plot their ratio. *p* values: Dunn's test. Quantification of Mira crescent size in the experiments indicated. (**D**) The NB was allowed to polarize in the absence (*upper row*) or presence of 25µM Y-27632 (middle and lower row) followed by colcemid arrest leading to an enlarged Mira crescent in treated cellls (white arrowheads). *upper row*: A colcemid arrested NB with normal Mira crescent (yellow arrowheads) was depolarized by 1µM LatA. Effect of LatA is visible with uniform cortical Baz signal. Mira was displaced into the cytoplasm. *middle row*: adding 1µM LatA leads to displacement of the enlarged Mira crescent in the cytoplasm. Mira was displaced into the cytoplasm. *Lower row:* adding 20µM ML-7 drives Mira into the cytoplasm (+8'). Upon ML-7 washout, Mira recovered to an enlarged crescent (+14', white arrowheads). (**E**). Colcemid arrested NBs was treated with 200µM Y-276322. Mira remains asymmetric even after 56min in the drug. LatA addition (5µM) abolishes that asymmetric bias and Mira is uniformly distributed on the membrane (1: *p*=0.000000002868; 2: p=0.000004013; 3: *p*=0.0000000853; 4: *p*=0.06884690; 5: *p*=0.39018501; 6: *p*=0.662765116). *Time* stamp: min. Labels as indicated. *BAC{mira::mcherry-MS2}* was the source of Mira::mCherry. Scale bar:10µm.

Figure supplements

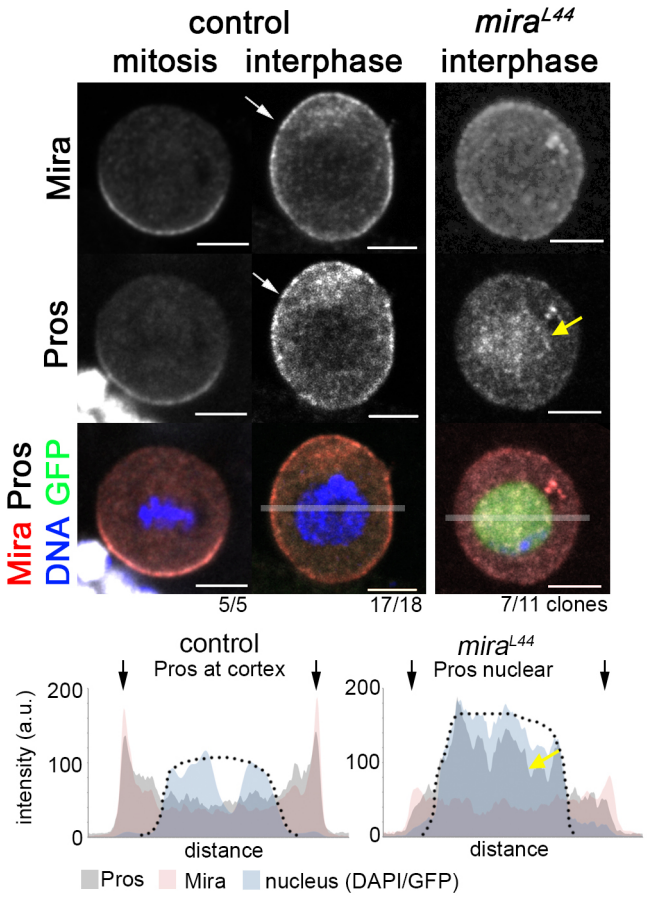

Figure 1 supplement 1

Figure 1 supplement 1. Uniform cortical Prospero depends on Miranda in interphase larval NBs. In w^{1118} brains, Mira and Pros form basal crescents in mitosis and both are cortical in interphase (arrow). In an interphase *mira*^{L44} NB (MARCM clone, GFP^{+}) cortical Mira and Pros are strongly reduced and Pros accumulates in the nucleus (yellow arrow). Transparent bars in merge interphase (control) and *mira*^{L44} indicate area used for plot profiles shown below. Pros and Mira are at the cortex (arrows) in the control and Pros is enriched in the nucleus in the mutant (yellow arrow). Parsed straight line: outline of cell. Dotted line: nucleus (based on DAPI, control and GFP (MARCM clone). Scale bar: 10µm.

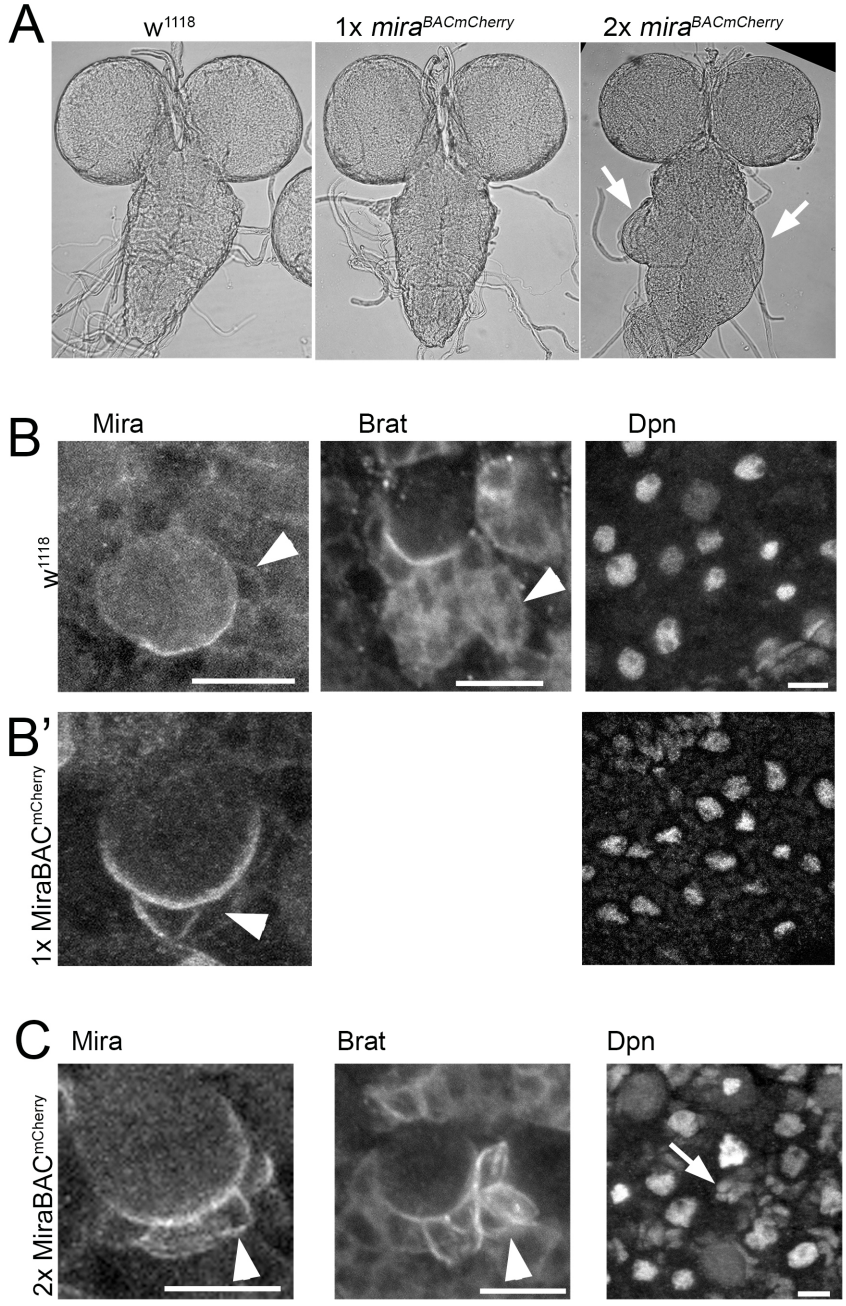

Fig 1 supplement 2

Figure 1 supplement 2. *mira*^{BACmCherry} rescues embryonic lethality of the loss of function allele *mira*^{L44} over the deficiency DF(3R)ora^{I9}. However, animals die during puparium formation, when *mira*^{BACmCherry} is the only source of Mira. (**A**) Brightfield images of fixed whole mount brain preparations. *w*^{1118} (control, n=5) a *mira*^{BACmCherry} brain over a wild type chromosome (1x *mira*^{BACmCherry}, *n=12*) and a brain from *mira*^{BACmCherry} Df(3R)ora^{I9} over a unrecombined *mira*^{BACmCherry} chromosome (2x *mira*^{BACmCherry}, *n=12*). 2x

825 *mira*^{BACmCherry} animals die as pharates. The ventral ganglion (VG) of these
826 brains is frequently overgrown (arrows). (**B**) In fixed *w*^{1118} brains Mira as well
827 as its cargo Brat are diffuse in the cytoplasm of NB daughter cells and
828 Deadpan (Dpn) staining is restricted to NB nuclei. (**B'**) *mira*^{BACmCherry} brains
829 are not overgrown, Mira is sometimes more stable at the cortex in a daughter
830 cell (arrowhead), but Dpn is normal. (**C**) In 2x *mira*^{BACmCherry} animals, Mira is
831 strongly cortical in several NB daughter cells and so is Brat (arrowheads). Dpn
832 is no longer restricted to NB nuclei but frequently found in clusters of smaller
833 nuclei close to NBs suggesting that Mira is stabilized at the cortex and fails to
834 release its cargo, inducing fate changes. mCherry is fused to the C-terminus
835 of Mira which was shown to be required for cargo release (Fuerstenberg et al.
836 1998; Matsuzaki et al. 1998).
837

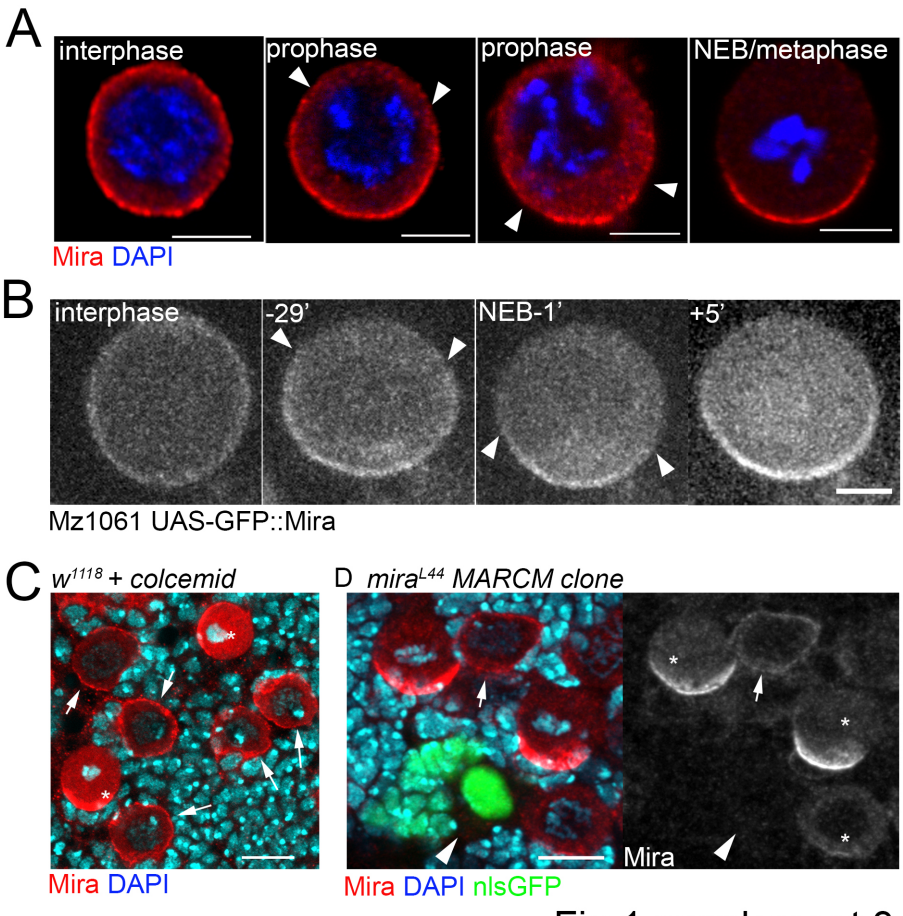

Fig 1 supplement 3

838

839 **Figure 1 supplement 3**. *Cortical Mira can be detected by antibody staining,*
840 *in UAS-GFP-Mira overexpressing NBs and upon colcemid treatment, but not in*

841 *interphase mira^{L44} loss of function clones*. (A) Antibody staining against Mira
842 performed on different fixed isolated NBs in primary cell culture. In this assay
843 Mira (red) is cortical in an interphase NBs (judged by DAPI, blue). In
844 prophase NBs, differently sized Mira "crescents" can be detected the ends of
845 which are labeled by arrowheads. In a metaphase NBs Mira forms a crescent
846 that appears larger than some of those seen in prophase NBs. (B) A living NB
847 in primary cell culture expressing Mira::GFP driven by Mz1061. GFP signal is
848 at the cortex in interphase, 29 min prior to NEB, GFP signal becomes cleared
849 apically (arrowheads) until most of the cortex is cleared 1min prior to NEB. 5
850 min after NEB a robust, larger crescent has formed. (C) Control brain treated
851 with 50µM colcemid for 30min and stained for Mira. Over condensed
852 chromatin in mitotic NBs demonstrates the effect of colcemid yet in all
853 interphase NBs Mira remains at the cortex. (D) Fixed brain containing an
854 interphase NB MARCM *mira^{L44}* clone surrounded by control NBs. In the clone
855 cortical Mira signal is gone (arrowhead) while present in a control interphase
856 NB (arrow). Asterisks: mitotic NBs. Scale bar 10µm.
857
858
859

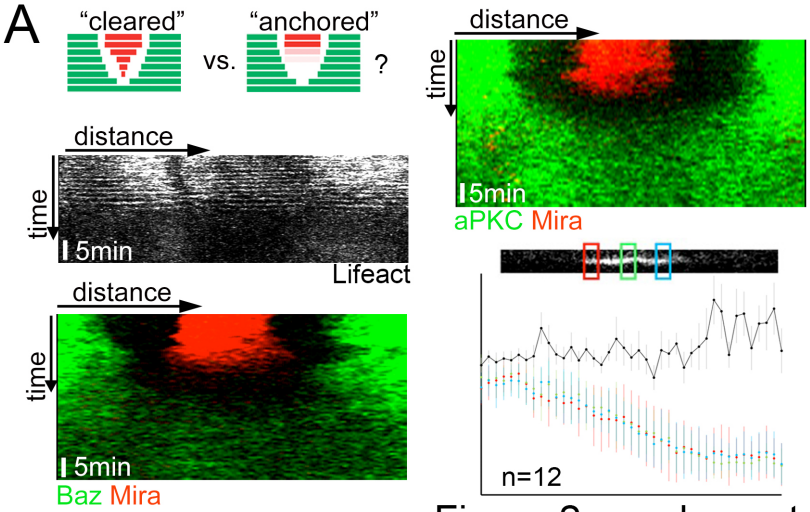

Figure 2 supplement

860
861 **Figure 2 supplement.** (**A**) Schematic depicting the expected kymograph
862 profile for *clearing* versus *anchoring*. Kymographs of colcemid arrested NBs
863 expressing Lifeact-Ruby, Baz::GFP and Mira::mCherry or aPKC::GFP and

Mira::mCherry (related to **Movie S4**) upon the addition of 5µM LatA. The equatorial perimeter of the NB was straightened out for each time point. Time scale bar: 5min. Plot of Mira decline upon LatA treatment of a colcemid arrested NB using 3 ROIs (positions as indicated). Black line shows ratio ROI3/ROI2 over time, which remains constant. (**B**) aPKC has similar localization dynamics to Baz during NB polarization (compare to Fig 1B). (**C**) Metaphase Baz::GFP NBs fixed and stained for aPKC. Fluorescence distribution plotted below. aPKC and Baz have almost identical distribution. Error bars: standard deviation. *BAC{mira::mcherry-MS2}* was the source of Mira::mCherry. Scale bar: 10µm.

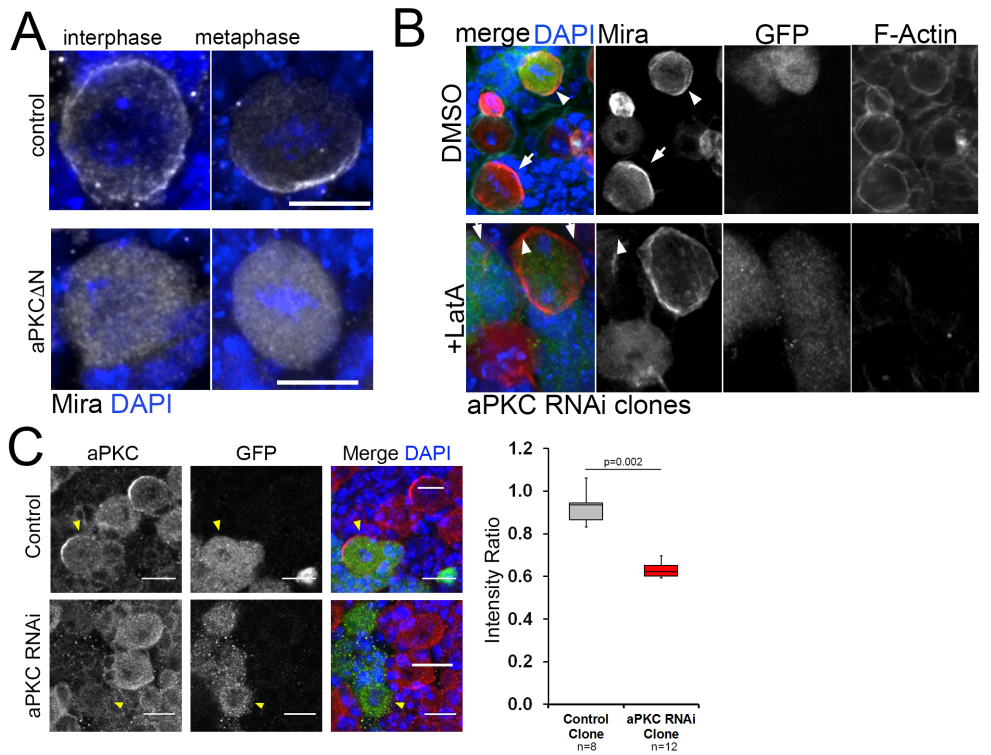

Fig 3 supplement

Figure 3 supplement. (**A**) Mira antibody staining on whole mount brains in a control NBs and in a NBs that expresses aPKC$^{\Delta N}$ by worniuGal4. Control: Mira is cortical in interphase (91% cortex, 9% cytopl., n=53), forms a crescent in metaphase (93% crescent, 7% cytopl., n=15) and is segregated to daughter cells in telophase (100%, n=9). aPKC$^{\Delta N}$: Mira is cytoplasmic in interphase (85% cytoplasm, 15% cortex, n=40) and metaphase (89%

cytopl., 11% crescent, n=15) but was rescued in telophase (100% cortical, n=12). (**B**) aPKC RNAi expressing flip out clones (GFP positive, arrowheads) and GFP negative control NBs (arrows) treated with DMSO or 5µM LatA and stained with an antibody against Mira and with Phalloidin. In GFP negative mitotic control NBs, Mira is in a crescent (DMSO) or cytoplasmic (LatA). Mira is cortical in DMSO as well as LatA treated mitotic aPKC RNAi NBs (100%, n=5, arrowheads). (**C**) aPKC is efficiently knocked down by RNAi in flip out clones. aPKC RNAi NBs have significantly less aPKC. Scale bar: 10µm.

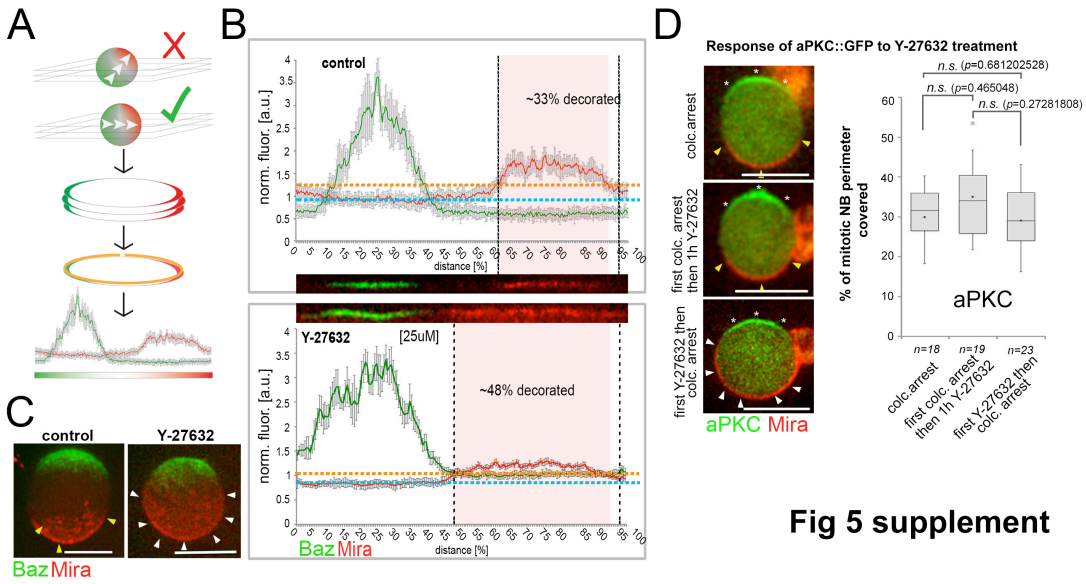

Fig 5 supplement

Figure 5 supplement. Standard used to quantify Mira crescent size. (**A**) Schematic of workflow. NBs that have a polarity axis parallel to the imaging plane are selected. 3-5 optical planes are collected covering 2-3µm of the equator of the NB. (**B**) Fluorescence is normalized against the cytoplasmic background and straightened line plots are derived from each section. The average background and the average standard deviation is determined. Signal: > avg. background plus two times the average standard deviation. (**C**) 3D projections of z-sections covering the entire NBs, ctrl vs. a NB that polarized in the presence of 25µM Y-27632. *BAC{mira::mcherry-MS2}* was the source of Mira::mCherry. Scale bar: 15µm.

Movie captions

Movie S1

Interphase cortical Miranda is removed at the onset of mitosis. Spinning disc confocal image of a neuroblast expressing Baz::GFP (red) and Mira::mCherry (green). For this and all subsequent videos maximum projection after a 3D Gaussian blur (FIJI, radius 8/.8/1) of 7 consecutive equatorial planes taken at 0.4µm spacing is shown. Z-stacks taken every minute. Time stamp: hh:mm.

Movie S2

Interphase cortical Miranda is removed at the onset of mitosis. Spinning disc confocal image of a neuroblast expressing aPKC::GFP (green) and Mira::mCherry (red). Z-stacks taken every minute. Time stamp: hh:mm.

Movie S3

Interphase cortical Miranda is actin independent. Spinning disc confocal image of a neuroblast expressing Baz::GFP (red) and Mira::mCherry (green) showing a control division before 1µM LatA was added. Z-stacks taken ~every minute. Z-stacks taken every minute. Time stamp: hh:mm.

Movie S4

Colcemid arrested NBs expressing aPKC::GFP and Mira::mCherry that were treated with 5µM LatA at the beginning of the recording at 16sec intervals. The cortex was straightened out and split at the apical pole such that aPKC::GFP appears right and left and Mira in the centre. Fluorescence profiles shown below. Note that Mira falls off homogenously from the cortex and becomes cytoplasmic at 5:36 (red arrowhead), while the detectable borders of cortical aPKC (green arrowheads) have not yet changed. Only from 7:12 onward aPKC rise above cytoplasmic levels where Mira was localized.

Movie S5

Myosin inhibition reversibly affects basal Mira anchoring in a polarized neuroblast. A colcemid arrested NB expressing Baz::GFP (green) and Mira::mCherry (red) in primary cell culture was treated with 20µM ML-7 which as washout when indicated. Left panel Baz::GFP, middle panel Mira::mCherry, right panel merge. Z-stacks taken every minute. Time stamp: mm:ss.

Movie S6

The effect of ML-7 on cortical Mira localization in mitosis can be delayed by overexpressing Sqh^{EE}. Mira::mCherry NBs (ctrl) and Mira::mCherry NBs co-expressing Sqh^{EE} (rescue) were co cultured in neighboring clots in the same dish and the effect of ML-7 on cortical Mira recorded. Z-stacks taken every two minutes. Time stamp: mm:ss.

Movie S7

Miranda remains at the cortex throughout the cell cycle in *apkc*^{k04603} mutant NBs. Spinning disc confocal image of an $apkc^{k04603}$ mutant NB, labeled with nlsGFP (green) expressing Mira::mCherry (white). Z-stacks taken every minute. Time stamp: hh:mm.

Movie S8

Control $mira^{mCherry}$ allele generated by CrispR/Cas9. Mira localizes to the interphase cortex, from where it is cleared before NEB. Then Mira re-localizes to a larger crescent. Therefore this allele and Mira::mCherry (BAC rescue) are undistinguishable in terms of Mira dynamics. This control further shows that the MS2 binding site in the BAC rescue construct do not interfere with Mira cortical dynamics. Time stamp: hh:mm.

Movie S9

Phosphomutant S96A allele of Mira tagged with mCherry at the C-terminus. Mira localizes uniformly to the interphase cortex. Shortly before NEB, S96A is

968 apically enriched, before being uniformly cortical after NEB and during
969 division. Time stamp: hh:mm.
970
971 **Movie S10**
972 Phosphomimetic S96D allele of Mira tagged with mCherry at the C-terminus.
973 S96D localizes to microtubules in interphase, but is asymmetric in mitois in
974 mitosis. Note the signal resembling subcortical microtubules in interphase
975 converging at the apical pole. After NEB a basal crescent is detectable. At
976 115:30 a z-stack spanning the entire NB was collected and the maximum
977 projection is frozen. After this 50µM colcemid was added to reveal if
978 $Mira^{S96D}$::mCherry binds to the cortex. Next frozen frame: similar stack after
979 30min in colc. Next frozen frame: 50 in colcemid – no cortical signal is
980 detectable. Last frozen frame 65min in colcemid. Time stamp: hh:mm. Scale
981 15µm.
982
983 **Movie 11**
984 Mira requires its BH motif for interphase cortical localization (see main text)
985 and basal localization in mitosis. The BH motif in Mira has been deleted by
986 gene editing and this Mira mutant tagged with mCherry at the C-terminus
987 (*mira*$^{\Delta BHmCherry}$). $Mira^{\Delta BH}$::mCherry when homozygous is found on the
988 interphase microtubule network and in the cytoplasm during mitosis. Time
989 stamp: hh:mm.
990
991 **Movie S12**
992 200µM Y-27632 induced uniform cortical Mira in mitosis localizes
993 independently of an intact actin network. A Baz::GFP and Mira::mCherry
994 expressing NBs was cultured in the presence of 200µM Y-27632, arrested
995 with colcemid. 5µM LatA was added after the first frame of the movie. LatA
996 induces loss of Baz asymmetry, yet Mira remains cortical. Z-stacks shown. Z
997 stacks taken every 2min.
998
999

Movie S13

Colcemid arrested NBs expressing Baz::GFP and Mira::mCherry, treated with 200µM Y-27632. Mira starts to become visibile ~36min after Y-27632 addition in this example, but remaind asymmetrically distributed, until LatA was added. Z-stacks shown. Z stacks taken every 2min.

Competing interest declaration

The authors declare no competing financial interests.

Author contribution

M.H., A.R., N.L. and J.J. designed and carried out experiments and interpreted the data and M.R.H., N.L. and J.J. wrote the manuscript that was agreed upon by all authors.